Environ Fluid Mech (2015) 15:235–250
DOI 10.1007/s10652-013-9306-3

ORIGINAL ARTICLE

Large-eddy simulation of turbulent flow in a densely built-up urban area

Seung-Bu Park · Jong-Jin Baik · Beom-Soon Han

Received: 22 February 2013 / Accepted: 14 August 2013 / Published online: 29 August 2013

Abstract Turbulent flow in a densely built-up area of Seoul, South Korea, is numerically investigated using the parallelized large-eddy simulation model. Based on the analysis of streamwise velocity and column-averaged vertical turbulent momentum flux, three areas of interest are selected: a downstream area of an apartment complex, an area behind high-rise buildings, and a park area. In the downstream area of the apartment complex, a large wake develops and a region of strong vertical turbulent momentum flux appears above the wake. At the height of maximum vertical turbulent momentum flux magnitude, all the four quadrant events occur in larger magnitude and contribute more to the vertical turbulent momentum transport than the averages in the main domain. In the area behind the high-rise buildings, fluctuating wakes and vortices are distinct flow structures around the top of the tallest building and updrafts induced by the flow structures appear as strong ejections just behind the high-rise buildings or farther downstream. While strong ejections are dominant at building-top heights, downdrafts along the windward walls of high-rise buildings are distinct below building-top heights and they induce high turbulent kinetic energy and winding flow around the high-rise buildings near the ground surface, transporting momentum downward and intermittently into nearby streets. In the park area located downstream in the main domain, turbulent eddies exist well above the ground surface, and the thickness of the interfacial region between low-speed air and high-speed air increases and complex turbulent flow appears in the interfacial region.

Keywords Turbulent flow · Large-eddy simulation · Ejection · Sweep · Wake · Turbulence coherent structure · Densely built-up urban area

1 Introduction

Flow in a densely built-up urban area is an important subject in fluid mechanics of the urban atmosphere because of its impacts on building- to city-scale wind environment and pollutant

S.-B. Park · J.-J. Baik (✉) · B.-S. Han
School of Earth and Environmental Sciences, Seoul National University, 1 Gwanak-ro, Gwanak-gu, Seoul 151-742, South Korea
e-mail: jjbaik@snu.ac.kr

dispersion as well as fluid-mechanical interest. However, flow in a densely built-up urban area with various shapes and arrangements of buildings is highly turbulent and this makes it very difficult to understand.

Previous studies of urban turbulent flow have been mainly focused on turbulent flow in relatively simple urban morphologies such as a street canyon and a cubical building array [1,2,4–7,11,15,16,21]. Rotach [21] analyzed measurement data of turbulence in and above a street canyon and emphasized the importance of sweep events for the exchange between the canyon air and the air of the roughness sublayer above. Cui et al. [2] also highlighted a major contribution of sweep events at the canyon rooftop height to vertical turbulent momentum transport based on large-eddy simulation (LES). Using an LES model, Kanda [7] showed that low-speed streaks and streamwise vortices appear above building arrays and turbulence coherent structures resemble those of smooth wall boundary layers. Furthermore, turbulence coherent structures (e.g., low- and high-speed streaks) above building arrays were found to affect flow fields within the building arrays [5,16]. Although important turbulence structures have been revealed by previous studies, a gap remains between the findings from idealized simulations and actual flow in a densely built-up urban area because spatial inhomogeneities in real urban morphologies induce complex flow structures. Xie et al. [23] investigated the effects of randomness in the obstacle height of an obstacle array on turbulence statistics using an LES model and found that tall buildings contribute much to the total surface drag and produce a lot of turbulent kinetic energy (TKE) with respect to their frontal area. This indicates that flow structures induced by spatial inhomogeneities in urban morphologies can be dominant over the typical flow structures that appear in wall boundary layers.

Nowadays, digital elevation models (DEM) enable the use of highly accurate urban morphology to simulate turbulent flow in a densely built-up urban area. Nakayama et al. [13] conducted LES of turbulent flow in an area of Tokyo and proposed a method to estimate aerodynamic roughness parameters for actual urban areas. Nakayama et al. [14] simulated turbulent flow in an urban area, with mesoscale model simulation data being used as turbulent inflows, and compared wind fluctuations and gust factors to observations. Letzel et al. [10] investigated pedestrian level ventilation in two neighborhoods in Hong Kong using an LES model. They showed that the isolated tall building might have a pronounced impact on ventilation both locally and downstream. These studies focus more on estimating aerodynamic parameters and validating the LES model rather than investigating turbulence structures generated by buildings of various shapes and arrangements.

This study aims to investigate characteristic turbulence structures that appear in a densely built-up urban area. For this, turbulent flow is simulated using an LES model with urban elevation data being used as bottom boundary. The LES model and simulation setup are described in sect. 2. In sect. 3, simulation results are presented and discussed. A summary and conclusions are given in sect. 4.

2 Model description and simulation setup

The parallelized LES model (PALM) developed at the Leibniz University of Hannover [9,18] is used in this study. The model is based on the implicitly filtered Boussinesq equations. The momentum equation and subgrid-scale (SGS) TKE equation are numerically solved using the third-order Runge–Kutta scheme for time integration and the second-order Piacsek and Williams [17] scheme for advection. The 1.5-order Deardorff [3] scheme is used to parameterize SGS turbulent fluxes. PALM is described in more detail in Letzel et al. [9].

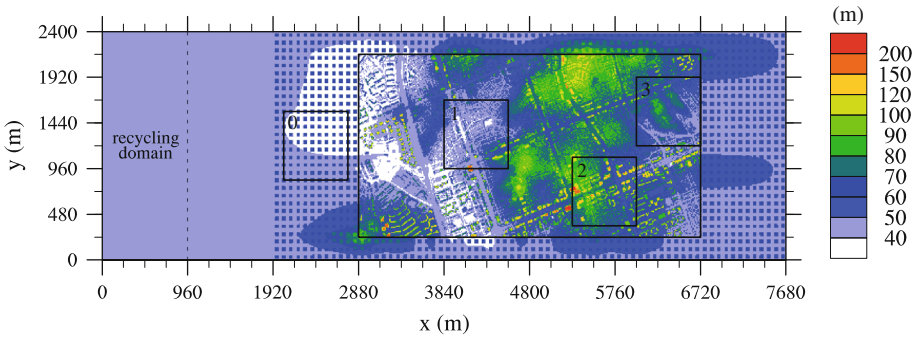

Fig. 1 Elevation field of ground and building top surfaces in the computational domain. The main domain and the areas of interest are indicated by inner rectangle with a *solid line* and *squares* with *solid lines*, respectively

To simulate turbulent flow in an actual urban morphology, gridded elevation data of a densely built-up urban area are used as the bottom boundary of the LES model. Figure 1 shows the elevation field of ground and building top surfaces in the computational domain. A densely built-up area of Seoul, South Korea, is selected. The main domain (3,840 m × 1,920 m, the inner rectangular region in Fig. 1) includes high-rise buildings, broad streets, residential areas, and a park. There are many high-rise buildings (two of them are higher than 150 m) on the Teheran Street from $(x, y) \sim$ (4440 m, 320 m) to $(x, y) \sim$ (6720 m, 1180 m) and apartment complexes around $(x, y) =$ (3360 m, 1320 m) and (3480 m, 360 m). There also exists one park (Samneung Park) around $(x, y) =$ (6300 m, 1560 m). The airborne light detection and ranging (LIDAR) data with a 1-m grid resolution are used to create coarser gridded elevation data with a 5-m grid resolution. In the selected area, the ground elevation varies from $\sim$ 30 to $\sim$ 90 m. The ground elevation is included in the gridded elevation data.

To apply a realistic boundary condition in the streamwise direction, the turbulence recycling method [8,12] is employed to generate turbulent inflow data for the main domain. A subdomain where turbulence is recycled is added in the upstream of the main domain. In the recycling domain, turbulent signals (perturbations from the horizontal average over the recycling domain) at the outflow boundary are repeatedly imposed at the inflow boundary, while initial mean vertical profiles (obtained from a precursor simulation) at the inflow boundary do not change during the simulation. In addition to the recycling domain, buffer regions are added around the lateral boundaries of the main domain. In the buffer regions, the variation of ground elevation is smoothed out toward the lateral boundaries of the computational domain to avoid a discontinuity in ground elevation and in-line arranged artificial buildings are located to prevent abrupt dissipation of turbulence there.

The size of the computational domain is 7,680 m in the x (east–west) direction, 2,400 m in the y (south–north) direction, and 1,020 m in the z (vertical) direction. The grid size in the x and y directions is 5 m. The grid size in the vertical direction is uniform with 5 m up to $z =$ 250 m and increases with an expansion ratio of 1.08 up to $z \sim$ 325 m, then being 10 m above that height. The number of grid points is 1,536 × 480 × 130. For velocity components and SGS TKE, the radiation boundary condition is applied at the east (outflow) boundary and the cyclic boundary condition is applied at the south and north boundaries. The Dirichlet boundary condition is applied at the top boundary. Westerly geostrophic wind ($u_g = 10\,\mathrm{m\,s^{-1}}$) is imposed in the model domain, and the Coriolis force induces anti-clockwise turning of mean wind direction downward in the boundary layer. At grid points closest to all the solid surfaces, the Monin–Obukhov (MO) similarity is employed in the momentum equation. The roughness

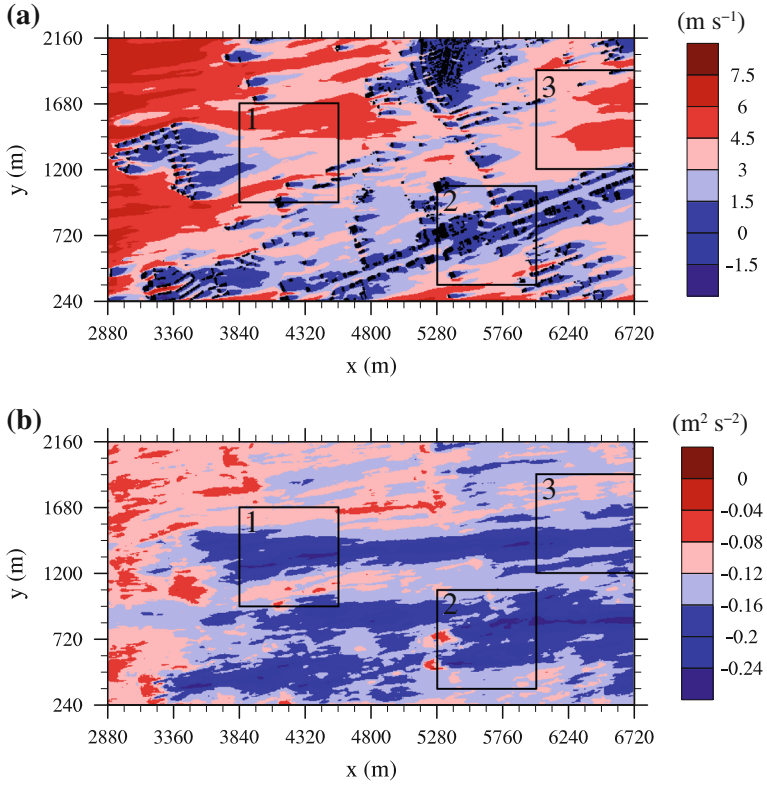

Fig. 2 Fields of **a** mean streamwise velocity at $z = 100$ m and **b** column-averaged vertical turbulent momentum flux. The areas of interest are indicated by *squares* with *solid lines*

length for momentum is 0.1 m. To obtain initial perturbations and mean vertical profiles in the recycling domain, a 2-h precursor simulation with a flat surface and cyclic boundary conditions at the lateral boundaries is conducted. Then, PALM is integrated for 2,400 s and the last 30-min simulation data are used for analysis.

3 Results and discussion

3.1 Turbulence statistics

Figure 2a shows the field of mean streamwise velocity $\bar{u}$ at $z = 100$ m. At $z = 100$ m, large wakes appear behind apartment complexes and are located around $(x, y) = (3600\,\text{m}, 1200\,\text{m})$, $(3840\,\text{m}, 420\,\text{m})$, and so on. An elongated area of low streamwise velocity, where small wakes are aligned and connected to each other, appears around the buildings on the Teheran Street. The mean streamwise velocity at $z = 100$ m is high in the Samneung Park due to the absence of high-rise buildings. To find areas where momentum is actively transported downward by turbulence, the vertical turbulent momentum flux at every grid point in the main domain is vertically integrated from $z_1 = 0$ m to $z_2 = 600$ m (∼boundary layer height) and then divided by the height difference $z_2 - z_1$. In this study, the boundary layer height is determined as the level where the mean streamwise velocity is about 95 % of

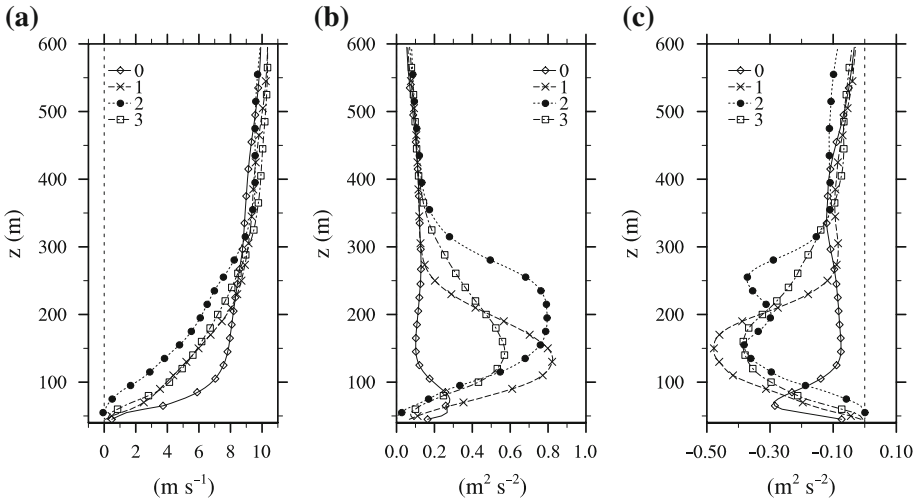

Fig. 3 Vertical profiles of area-averaged **a** mean streamwise velocity, **b** vertical velocity variance, and **c** vertical turbulent momentum flux in the four areas

the free stream velocity ($\bar{u}$ averaged between $z = 900$ and 1,000 m). Figure 2b shows the field of column-averaged vertical turbulent momentum flux $\frac{1}{(z_2-z_1)}\int_{z_1}^{z_2} \overline{u'w'}dz$. u' and w' denote deviations from the time-averaged (mean) streamwise velocity $\bar{u}$ and vertical velocity $\bar{w}$, respectively. The magnitude of column-averaged vertical turbulent momentum flux is large behind apartment complexes and the two high-rise buildings on the Teheran Street. The two areas are selected as the areas of interest (denoted by area 1 and area 2, respectively). The regions of large-magnitude column-averaged vertical turbulent momentum flux extend downstream. Although there are no high-rise buildings in the Samneung Park area, the magnitude of column-averaged vertical turbulent momentum flux is quite large there. Thus, the area around the Samneung Park is also selected as the area of interest (denoted by area 3). One area located upstream of the main domain (denoted by area 0) is selected to compare turbulence statistics in the three areas of interest to upstream turbulence statistics (Fig. 1). Column-averaged vertical mean momentum flux is also calculated. Its magnitude averaged over the main domain (0.37) is larger than the magnitude of column-averaged vertical turbulent momentum flux (−0.16) due to the inhomogeneous urban morphology.

The vertical profiles of mean streamwise velocity, vertical velocity variance, and vertical turbulent momentum flux averaged over the four areas are plotted in Fig. 3. The mean streamwise velocity below $z \sim 200$ m is higher in the upstream area (area 0) than in the other three areas (area 1, area 2, and area 3). The magnitudes of vertical velocity variance and vertical turbulent momentum flux in the three areas are overall much larger than those in the upstream area, indicating an enhancement of turbulence in a densely built-up urban area. The vertical velocity variance in area 1 has a maximum value at $z \sim 130$ m, slightly above the average height of upstream apartment buildings. The magnitude of vertical velocity variance in area 2 is also large at the top heights of high-rise buildings. The vertical turbulent momentum flux in area 1 has a maximum magnitude at $z \sim 150$ m, and that in area 2 has two peaks at $z \sim 150$ and 250 m. The mean streamwise velocity below $z \sim 300$ m is lower in area 2 than in the other areas due to dense high-rise buildings. In area 3, the vertical turbulent momentum flux has a maximum magnitude at $z \sim 150$ m and the shape of the

vertical profile is similar to that averaged over the main domain (not shown). Based on the turbulence statistics, two analysis heights (150 and 250 m) are selected.

Figure 4 shows the field of the joint probability density function (PDF) of u' and w' and the field of $u'w'$ multiplied by the joint PDF at $z = 150$ m in the main domain, 150 m in area 1, and 250 m in area 2. Dashed lines of equal $|u'w'|$ ($2\,\mathrm{m^2\,s^{-2}}$) are added in Fig. 4 to indicate the strength of turbulent events. The joint PDF of u' and w' is defined as $f_{u',w'}(a_i, a_j) = P[a_i - 0.5\Delta a < u' \leq a_i + 0.5\Delta a,\ a_j - 0.5\Delta a < w' \leq a_j + 0.5\Delta a]$ [16]. The number in each direction (N) and spacing (Δa) of bins used to calculate the joint PDF are 50 and 0.2, respectively. Note that the sum of all joint PDFs $\sum_{i=1}^{N}\sum_{j=1}^{N} f_{u',w'}(a_i, a_j)$ is one. The instantaneous vertical turbulent momentum flux $u'w'$ can be classified into four quadrants: outward interaction ($u'_+ w'_+$), ejection ($u'_- w'_+$), inward interaction ($u'_- w'_-$), and sweep ($u'_+ w'_-$) [19]. The joint PDF and $u'w'$ multiplied by the joint PDF illustrate the frequency of the four turbulent events and their contribution to vertical turbulent momentum flux, respectively.

The results at $z = 150$ m in the main domain show a typical pattern, that is, momentum is transported downward mostly by ejections and sweeps in the atmospheric boundary layer (Fig. 4d). The results at other heights in the main domain show similar patterns. The field of joint PDF and the field of $u'w'$ multiplied by the joint PDF at $z = 150$ m in area 1 show that stronger turbulent events occur more frequently at all quadrants than the average pattern in the main domain, inducing stronger vertical turbulent momentum flux at that height (Fig. 3c). The joint PDF field at $z = 250$ m in area 2 illustrates the effects of high-rise buildings and wakes behind them. The center of joint PDF moves from the origin to the fourth quadrant and the elliptical shape extends more to the second quadrant, indicating that sweeps occur more frequently and ejections become stronger than the average pattern in the main domain (Fig. 4a). The role of ejections in the vertical turbulent momentum transport can be confirmed again in the field of $u'w'$ multiplied by the joint PDF (Fig. 4f). In the downstream of the apartment complex, all the quadrant events contribute to the vertical turbulent momentum flux more than those in the main domain (Fig. 4e). In the area behind the high-rise buildings, on the other hand, only ejections become stronger (Fig. 4f). This seems to be related to the wakes and vortices that appear behind the high-rise buildings. In contrast to the fields of joint PDF and $u'w'$ multiplied by the joint PDF in area 2 at $z = 250$ m, those at $z = 150$ m are similar to the fields at $z = 150$ m in the main domain (not shown).

3.2 Turbulent flow behind an apartment complex

Figure 5 shows the fields of vertical turbulent momentum flux, instantaneous streamwise velocity at $t = 1{,}965$ s, and $\mathrm{sgn}(w') \cdot \max(0, -u'w')$ at $t = 1{,}965$ s in the x–z plane ($y = 1257.5$ m). The contours of mean or instantaneous streamwise velocity of $5\,\mathrm{m\,s^{-1}}$ are added. The quantity $\mathrm{sgn}(w') \cdot \max(0, -u'w')$ extracts ejection ($u'_- w'_+$) and sweep ($u'_+ w'_-$) events among the four quadrant events, and ejection and sweep events correspond to positive and negative values of the quantity, respectively [15]. The magnitude of vertical turbulent momentum flux is large just behind each apartment building due to locally generated turbulent eddies. There appears a large region of strong vertical turbulent momentum flux farther downstream of the apartment complex. Strong vertical momentum transport events usually occur around an interface between low-speed air and high-speed air, and the interface can be captured by plotting interfacial streamwise velocity [16]. Even in this kind of complex turbulent flow, the interface between low-speed air and high-speed air can be captured simply

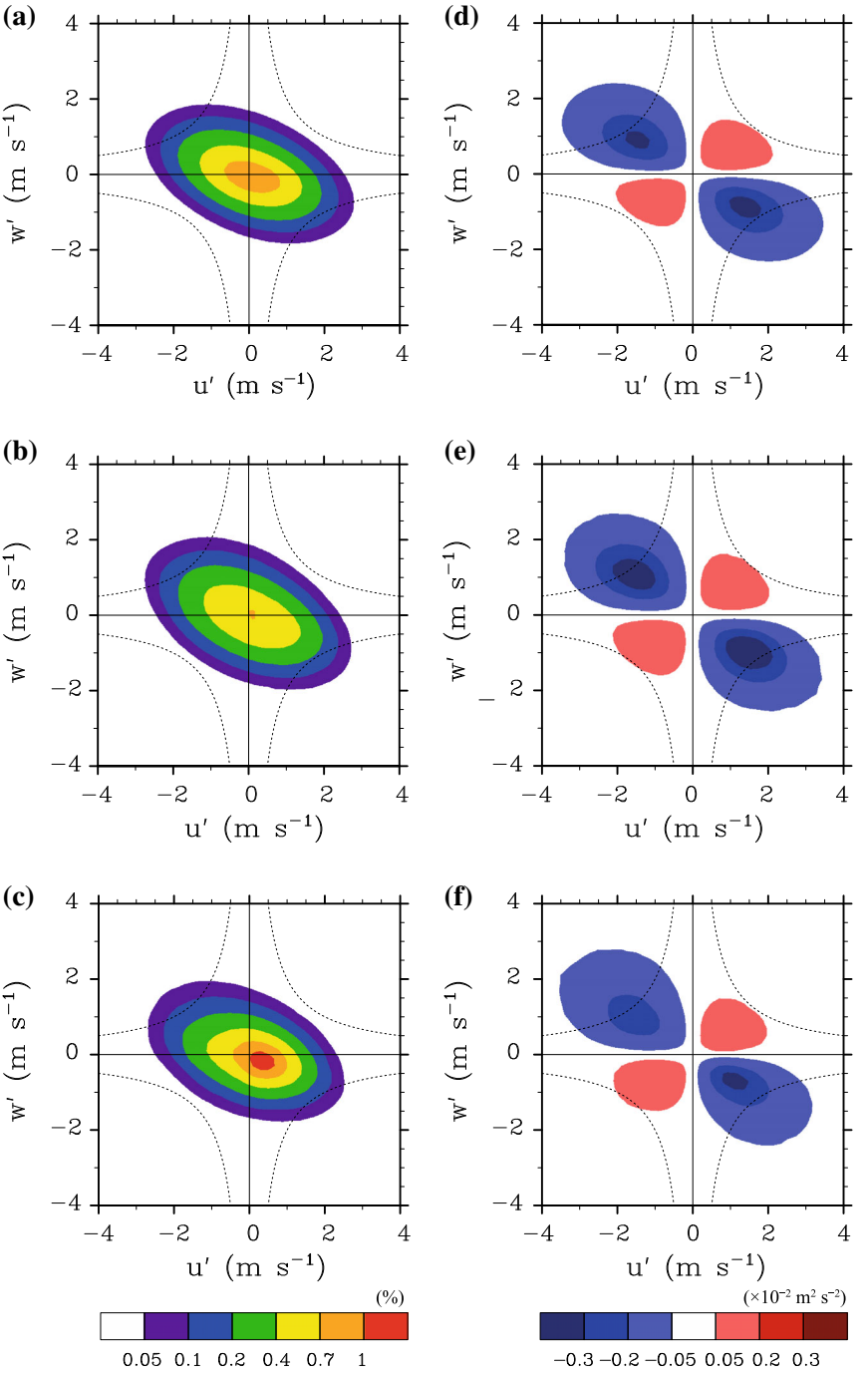

Fig. 4 Fields of the joint probability density function of u' and w' at **a** $z = 150$ m in the main domain, **b** $z = 150$ m in area 1, and **c** $z = 250$ m in area 2 and $u'w'$ multiplied by the joint probability density function at **d** $z = 150$ m in the main domain, **e** $z = 150$ m in area 1, and **f** $z = 250$ m in area 2. *Dashed lines* of equal $|u'w'|$ ($2\,\mathrm{m^2\,s^{-2}}$) are added

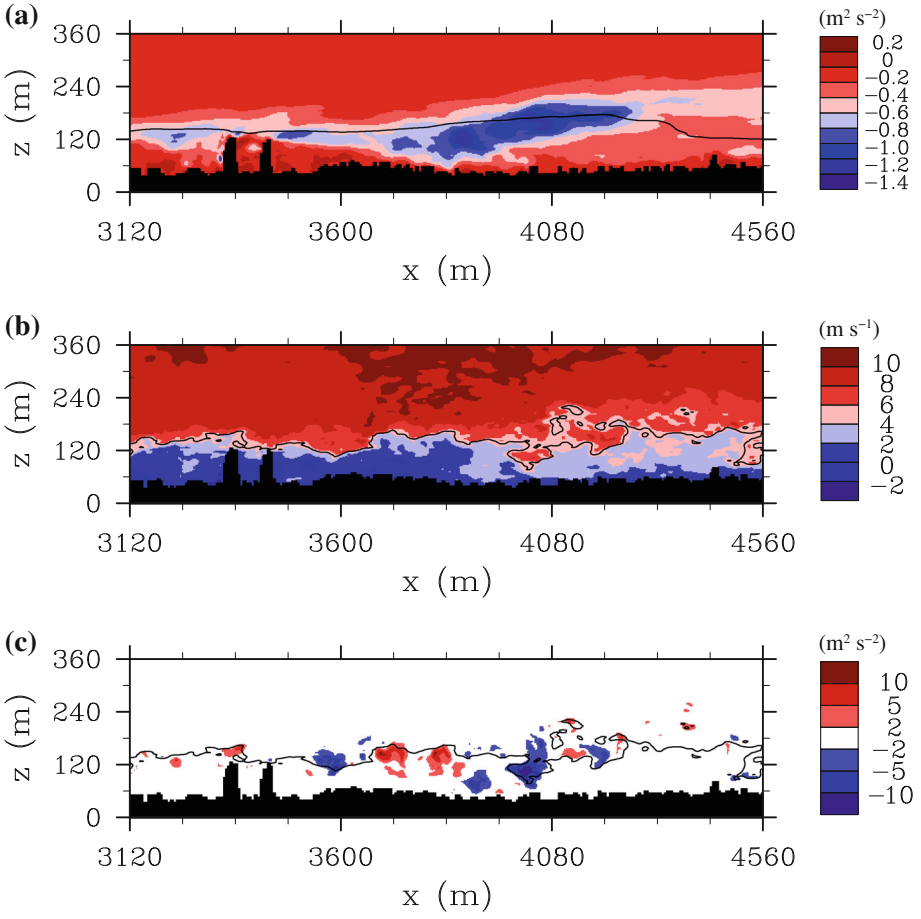

Fig. 5 Fields of **a** vertical turbulent momentum flux, **b** instantaneous streamwise velocity at $t = 1{,}965$ s, and **c** $\mathrm{sgn}(w') \cdot \max(0, -u'w')$ at $t = 1{,}965$ s in the x–z plane ($y = 1257.5$ m). The contours of streamwise velocity (5 m s^{-1}) are added

by plotting the contours of streamwise velocity (5 m s^{-1} in the present simulation) and strong vertical momentum transport events such as ejections and sweeps occur along the interface (Fig. 5c). As going downstream from the apartment complex, an interfacial region around the interface (e.g., $2 < u < 6$ m s^{-1}) extends downward and it also extends upward ($x > 3,840$ m). In the vertically extended interfacial region, overall magnitude and scale of turbulent eddies increase and the increase might be related to the large region of strong vertical turbulent momentum flux farther downstream. It is also possible that the large wake (Fig. 2a), which appears as a result of combined smaller wakes, induces spanwise converging flow around the wake and the converging flow results in strong vertical turbulent momentum flux above the wake.

Conditionally averaged streamwise velocity perturbation and velocity perturbation vector fields corresponding to ejections and sweeps in area 1 are shown in Fig. 6. Local minimum points of $u'w'$ in the x–y plane ($z = 150$ m) satisfying a certain criterion (e.g., $u'w' < -2$ m^2 s^{-2}) are collected, and the data around the minimum points are transformed to a new coordinate (x', y', z) and averaged to extract characteristic flow structures of turbulent

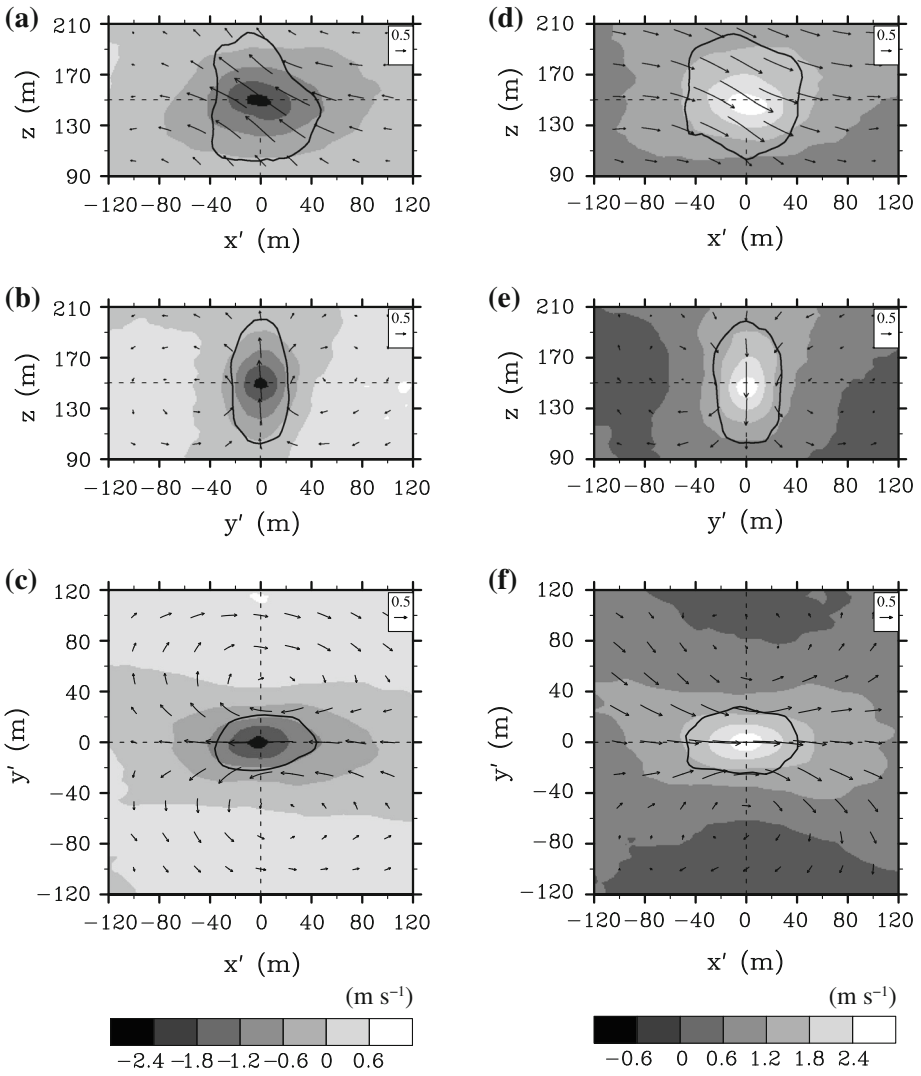

Fig. 6 Conditionally averaged u' and velocity perturbation vector (u', v', w') fields of ejections in the **a** x'–z plane ($y' = 0$ m), **b** y'–z plane ($x' = 0$ m), and **c** x'–y' plane ($z = 150$ m) and the same fields of sweeps in the **d** x'–z plane ($y' = 0$ m), **e** y'–z plane ($x' = 0$ m), and **f** x'–y' plane ($z = 150$ m). These are for area 1. The contours of vertical velocity (0.5 m s^{-1} for ejections and -0.5 m s^{-1} for sweeps) are added

eddies [16]. At $z = 150$ m in area 1, ejections and sweeps are comparable in frequency and magnitude (Fig. 4e) and the conditionally averaged fields composed of ejections and sweeps do not show distinct structures due to their opposite directions. To see distinct structures, samples of ejections and those of sweeps are collected and averaged separately by applying an additional criterion (a sign of vertical velocity perturbation). The velocity perturbation vector (u', v', w') instead of (u, v, w) are plotted to illustrate the relative motion of turbulent eddies with respect to the mean flow. The conditionally averaged flow fields show that negative and positive streamwise velocity perturbations are well correlated with updrafts (ejections) and downdrafts (sweeps), respectively. The flow structure of ejections is similar to the typical

turbulence coherent structure above cubical building arrays [1,4,16], and that of sweeps is similar to the turbulence coherent structures at the top of a plant canopy [22] or a cubical building array [16]. This indicates that turbulence structures behind the apartment complex are affected by the wall boundary layer turbulence and mixing layer turbulence [20].

3.3 Turbulent flow behind high-rise buildings

Figure 7 shows the fields of vertical turbulent momentum flux in the x–z plane ($y = 552.5$ m), instantaneous vertical velocity at $t = 2{,}385$ s in the x–y plane ($z = 250$ m), streamwise vorticity at $t = 2{,}385$ s in the x–y plane ($z = 250$ m), and $\mathrm{sgn}(w') \cdot \max(0, -u'w')$ at $t = 2{,}385$ s in the x–y plane ($z = 250$ m). The contours of mean or instantaneous streamwise velocity of 5 m s^{-1} are added. Wakes behind the high-rise buildings and their fluctuating (south and north) features are captured by the contours of streamwise velocity. The fluctuating turbulent wakes are well-known fluid phenomena (usually occurring behind a cylinder), and they seem to be related to downstream ejections. At $z = 250$ m (near the top of the tallest building), turbulent eddies that penetrate into the building wakes induce spanwise and vertical vortices behind the buildings and parts of the vortices become streamwise vortices due to wind shear (Fig. 7c). Strong updrafts appear with the streamwise vortices in the streamwise-elongated wakes and parts of the wakes are detached and advected downstream. Ejections are dominant in both the building-connected wakes and detached wakes, contributing to vertical turbulent momentum transport in the downstream of the buildings (Fig. 7d).

Conditionally averaged vertical velocity and velocity perturbation vector fields in area 2 are shown in Fig. 8. As shown in Fig. 4f, ejections are dominant over sweeps at $z = 250$ m in area 2. Thus, ejections are distinct in the conditionally averaged fields without any additional criterion. In contrast to ejections in area 1 (Fig. 6a–c), ejections in area 2 exhibit a vertically extended shape with strong updrafts, indicating that updraft-induced flow structures behind the high-rise buildings are dominant in transporting momentum downward. The structure of wakes behind the high-rise buildings is also well captured by the contours of streamwise velocity 5 m s^{-1} in Fig. 8a.

Figure 9 shows the fields of TKE and mean velocity vector and instantaneous wind speed and velocity vector ($t = 2{,}105$ s) at $z = 90$ m. In area 2, the west part of the Teheran Street has high ground elevation (~ 80 m) and the mean velocity there is low at $z = 90$ m. Except for the high ground elevation region, the mean flow on the Teheran Street blows in the street direction. On the Teheran Street, high-rise buildings exist and they induce downdrafts along their windward walls and updrafts along their leeward walls. The downdrafts along the windward walls induce winding flow and high TKE near the ground surface, and the momentum transported by the downdrafts is transported into nearby streets (Fig. 9a). This kind of flow system is more distinct in the instantaneous flow field. Around the building at $(x, y) \sim (5670\,\mathrm{m}, 870\,\mathrm{m})$, a high wind speed pattern, which is mostly induced by downdrafts at the windward wall of the building, and an extension of high wind speed to the Teheran Street are distinct (Fig. 9b). Thus, not only the direction of street but also the arrangement of high-rise buildings on the street is important to the direction and strength of wind on the street.

3.4 Turbulent flow in a park area

As indicated by the streamwise-directed band (at $y \sim 1{,}440$ m) in Fig. 2b, the column-averaged vertical turbulent momentum flux in area 3 is not negligible despite the absence of high-rise buildings. This is attributed to the vertical growth of internal boundary layer.

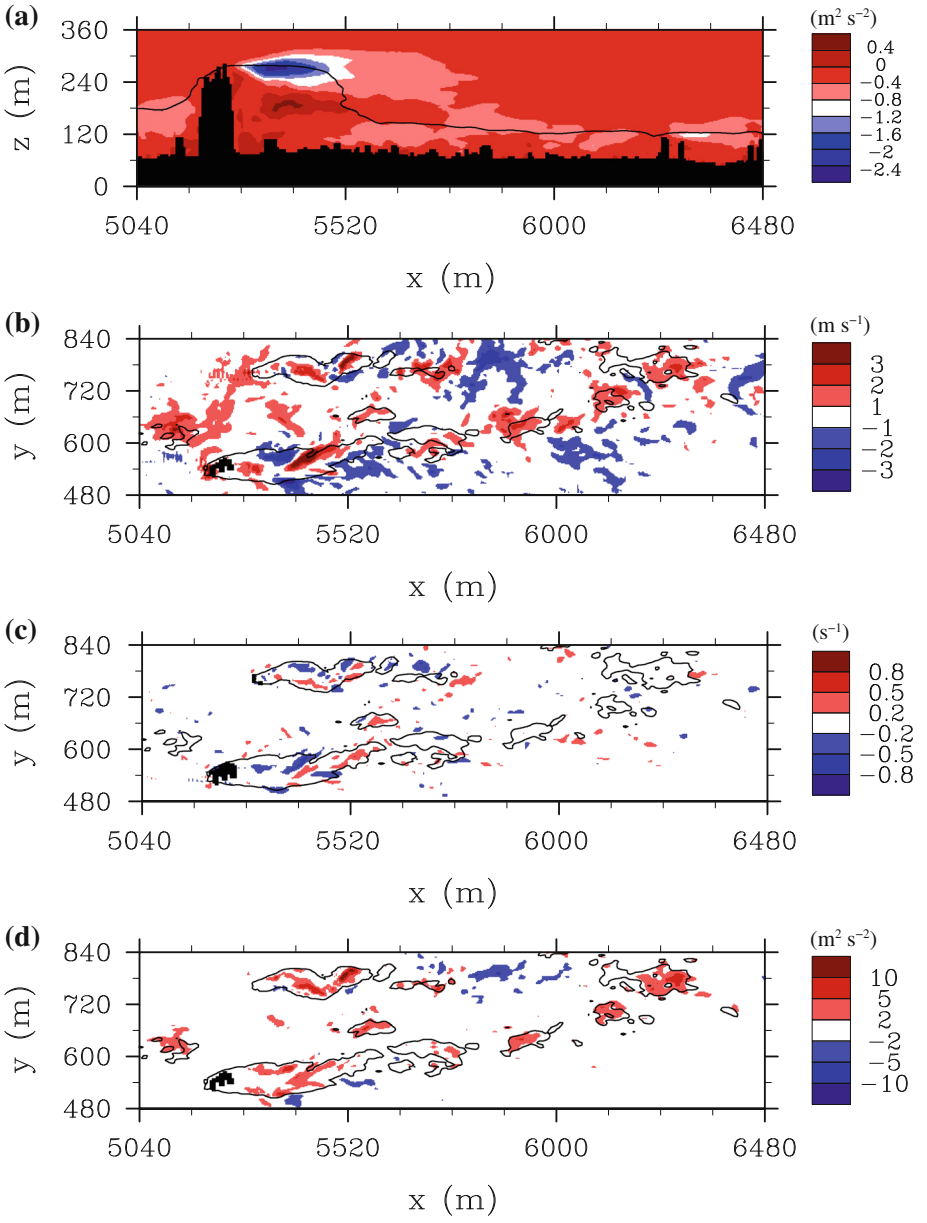

Fig. 7 Fields of **a** vertical turbulent momentum flux in the x–z plane ($y = 552.5$ m), **b** instantaneous vertical velocity at $t = 2,385$ s in the x–y plane ($z = 250$ m), **c** streamwise vorticity at $t = 2,385$ s in the x–y plane ($z = 250$ m), and **d** $\mathrm{sgn}(w') \cdot \max(0, -u'w')$ at $t = 2,385$ s in the x–y plane ($z = 250$ m). The contours of streamwise velocity (5 m s^{-1}) are added

Figure 10 shows the fields of vertical turbulent momentum flux, instantaneous streamwise velocity at $t = 2{,}065$ s, and $\mathrm{sgn}(w') \cdot \max(0, -u'w')$ at $t = 2{,}065$ s in the x–z plane ($y = 1{,}440$ m). The contours of streamwise velocity of 5 m s^{-1} and those of 8 m s^{-1} are added. As going downstream, the magnitude of vertical turbulent momentum flux decreases

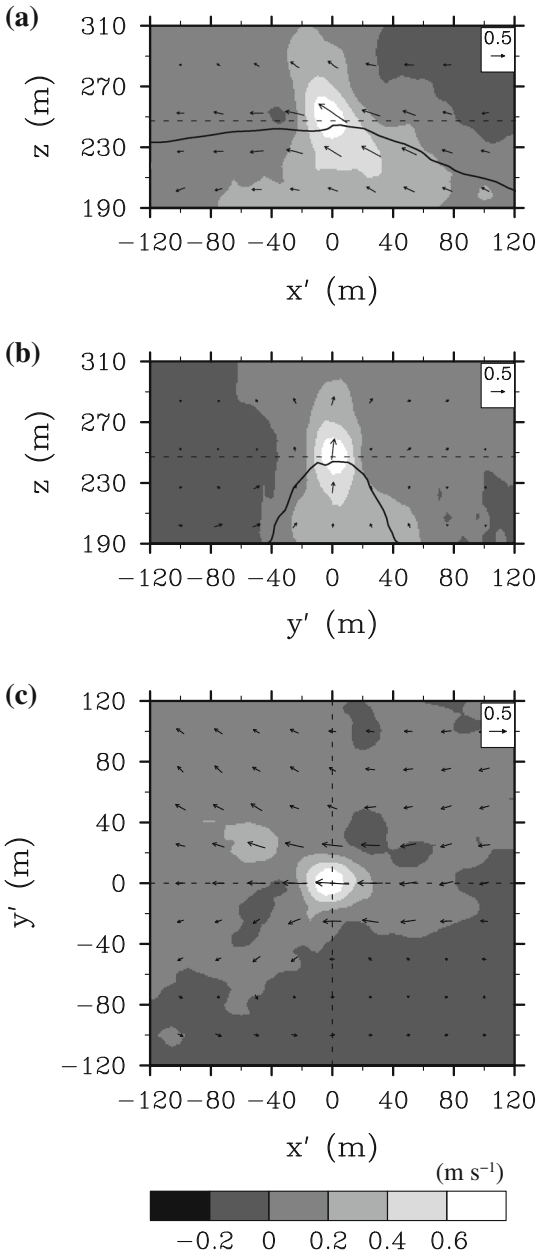

Fig. 8 Conditionally averaged w and velocity perturbation vector (u', v', w') fields in the **a** x'–z plane ($y' = 0$ m), **b** y'–z plane ($x' = 0$ m), and **c** x'–y' plane ($z = 250$ m). These are for area 2. The contours of streamwise velocity (5 m s^{-1}) are added

near the ground but the internal boundary layer develops upward as indicated by the vertical turbulent momentum flux field. As a result, the magnitude of vertical turbulent momentum flux at high levels increases toward downstream (Fig. 10a). As the internal boundary layer extends vertically toward downstream, the interface between low-speed air and high-speed air becomes less distinct while the interfacial region (e.g., $5 < u < 8$ m s^{-1}) broadens in the vertical direction. As shown in Fig. 10c, ejections and sweeps appear at higher levels than those in the upstream area (Fig. 5c). Some ejections and sweeps appear around the

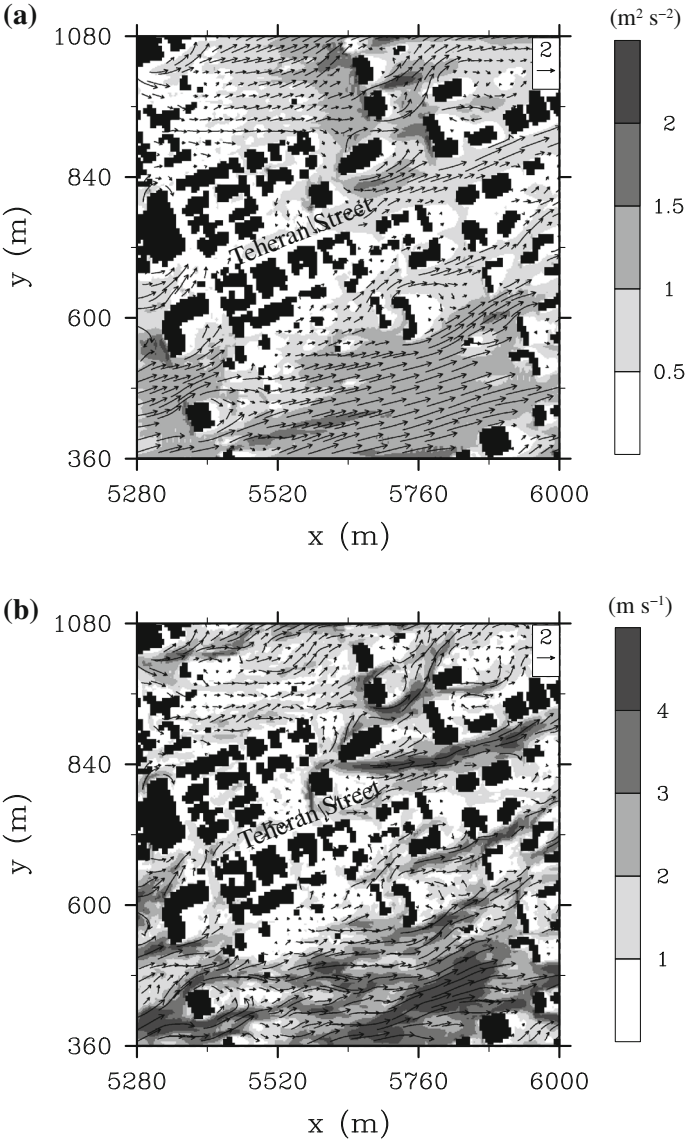

Fig. 9 Fields of **a** turbulent kinetic energy and mean velocity vector and **b** instantaneous wind speed and velocity vector ($t = 2,105$ s) at $z = 90$ m

interface of streamwise velocity 5 m s^{-1}, and others appear around the new higher interface of streamwise velocity 8 m s^{-1}. Figure 10c indicates that the distribution of turbulent eddies in area 3 is complex despite the absence of high-rise buildings.

4 Summary and conclusions

Turbulent flow in a densely built-up area of Seoul was simulated using an LES model with urban elevation data. Based on streamwise velocity and column-averaged vertical turbulent

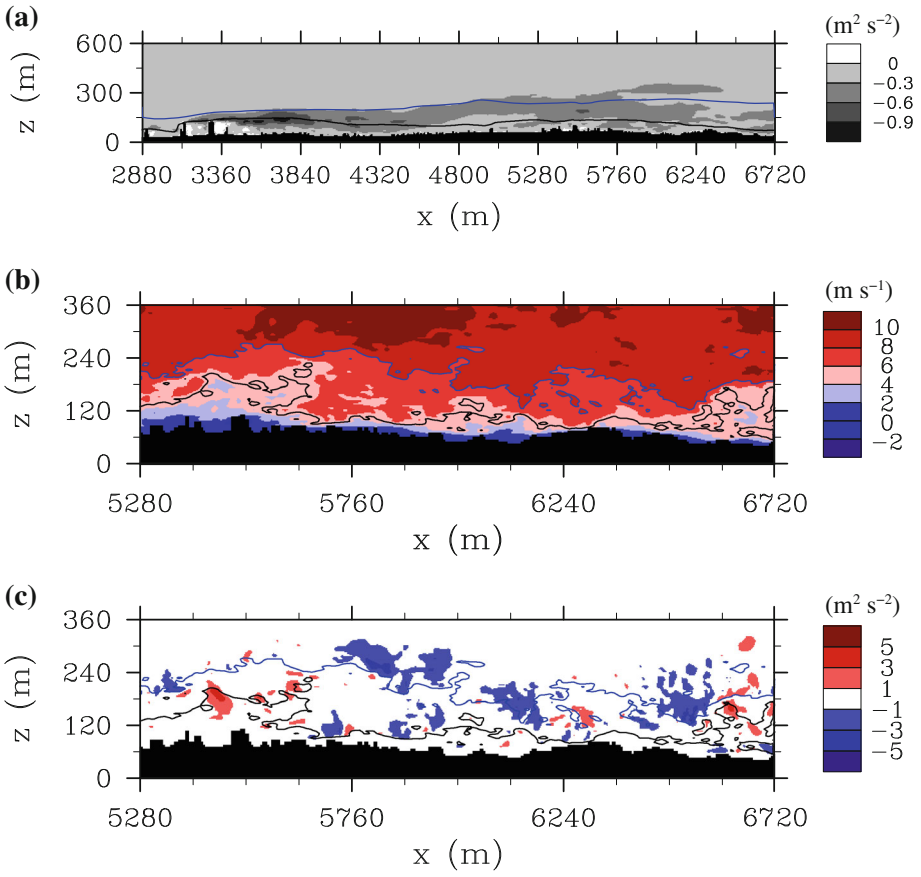

Fig. 10 Fields of **a** vertical turbulent momentum flux, **b** instantaneous streamwise velocity at $t = 2{,}065$ s, and **c** $\mathrm{sgn}(w') \cdot \max(0, -u'w')$ at $t = 2{,}065$ s in the x–z plane ($y = 1{,}440$ m). The contours of streamwise velocity of 5 m s^{-1} (*black*) and those of 8 m s^{-1} (*blue*) are added

momentum flux, three areas of interest were selected: a downstream area of an apartment complex, an area behind high-rise buildings, and a park area. In the downstream area of the apartment complex, all the four quadrant events at $z = 150$ m become stronger and contribute more to the vertical turbulent momentum transport than the averages in the main domain. Wakes behind apartment buildings are combined to form a large wake, and a large region of strong vertical turbulent momentum flux appears above the wake. Conditionally averaged fields show typical structures of ejections and sweeps. In the area behind the high-rise buildings, fluctuating wakes and vortices appear. Streamwise vortices occur with strong updrafts behind the high-rise buildings and updrafts-induced ejections are dominant in the building-connected and detached wakes. The joint PDF field at $z = 250$ m shows dominant ejections. Conditionally averaged fields also show strong ejections combined with updrafts along the leeward walls of the high-rise buildings. The high-rise buildings induce strong downdrafts along their windward walls and the downdrafts transport momentum downward. Mean and instantaneous fields show high TKE and strong winding flow around the high-rise buildings near the ground surface. The downdrafts induce intermittent flow into nearby streets, resulting in mean flow directed to the street direction. In the park area, the internal boundary

layer is developed more vertically than in the upstream area, inducing non-negligible vertical turbulent momentum flux at high levels. As turbulent eddies appear at higher levels, the distribution pattern of ejections and sweeps in the park area becomes complex despite the absence of high-rise buildings.

In this study, westerly geostrophic wind was considered. Recently, LES-simulated turbulence and scalar dispersion in urban areas were reported to be more accurate when data from a mesoscale model or measurement at a high tower are used as inflow data [14,24]. Further study with the LES model coupled to a mesoscale model is expected to show more realistic turbulent flow in a densely built-up urban area. Along with the simulation of realistic urban flow, an in-depth investigation of turbulence coherent structures behind typical urban buildings is required to better understand complex turbulent flow in a densely built-up urban area.

Acknowledgments The authors thank two anonymous reviewers for providing valuable comments on this work. This work was supported by the National Research Foundation of Korea (NRF) grant funded by the Korea Ministry of Education, Science and Technology (MEST) (No. 2012-0005674) and also supported by the Brain Korea 21 Project (through the School of Earth and Environmental Sciences, Seoul National University).

References

1. Coceal O, Dobre A, Thomas TG (2007) Unsteady dynamics and organized structures from DNS over an idealized building canopy. Int J Climatol 27:1943–1953
2. Cui Z, Cai XM, Baker CJ (2004) Large-eddy simulation of turbulent flow in a street canyon. Quart J R Meteor Soc 130:1373–1394
3. Deardorff JW (1980) Stratocumulus-capped mixed layers derived from a three-dimensional model. Bound Layer Meteor 18:495–527
4. Inagaki A, Kanda M (2010) Organized structure of active turbulence over an array of cubes within the logarithmic layer of atmospheric flow. Bound Layer Meteor 135:209–228
5. Inagaki A, Castillo MCL, Yamashita Y, Kanda M, Takimoto H (2012) Large-eddy simulation of coherent flow structures within a cubical canopy. Bound Layer Meteor 142:207–222
6. Kanda M, Moriwaki R, Kasamatsu F (2004) Large-eddy simulation of turbulent organized structures within and above explicitly resolved cube arrays. Bound Layer Meteor 112:343–368
7. Kanda M (2006) Large-eddy simulations on the effects of surface geometry of building arrays on turbulent organized structures. Bound Layer Meteor 118:151–168
8. Kataoka H, Mizuno M (2002) Numerical flow computation around aeroelastic 3D square cylinder using inflow turbulence. Wind Struct 5:379–392
9. Letzel MO, Krane M, Raasch S (2008) High resolution urban large-eddy simulation studies from street canyon to neighbourhood scale. Atmos Environ 42:8770–8784
10. Letzel MO, Helmke C, Ng E, An X, Lai A, Raasch S (2012) LES case study on pedestrian level ventilation in two neighbourhoods in Hong Kong. Meteor Z 21:575–589
11. Louka P, Vachon G, Sini JF, Mestayer PG, Rosant JM (2002) Thermal effects on the airflow in a street canyon—Nantes'99 experimental results and model simulations. Water Air Soil Pollut F 2:351–364
12. Lund TS, Wu X, Squires KD (1998) Generation of turbulent inflow data for spatially-developing boundary layer simulations. J Comput Phys 140:233–258
13. Nakayama H, Takemi T, Nagai H (2011) LES analysis of the aerodynamic surface properties for turbulent flows over building arrays with various geometries. J Appl Meteor Climatol 50:1692–1712
14. Nakayama H, Takemi T, Nagai H (2012) Large-eddy simulation of urban boundary-layer flows by generating turbulent inflows from mesoscale meteorological simulations. Atmos Sci Lett 13:180–186
15. Park SB, Baik JJ, Raasch S, Letzel MO (2012) A large-eddy simulation study of thermal effects on turbulent flow and dispersion in and above a street canyon. J Appl Meteor Climatol 51:829–841
16. Park SB, Baik JJ (2013) A large-eddy simulation study of thermal effects on turbulence coherent structures in and above a building array. J Appl Meteor Climatol 52:1348–1365
17. Piacsek SA, Williams GP (1970) Conservation properties of convection difference schemes. J Comput Phys 6:392–405

18. Raasch S, Schröter M (2001) PALM—a large-eddy simulation model performing on massively parallel computers. Meteor Z 10:363–372
19. Raupach MR (1981) Conditional statistics of Reynolds stress in rough-wall and smooth-wall turbulent boundary layers. J Fluid Mech 108:363–382
20. Raupach MR, Finnigan JJ, Brunet Y (1996) Coherent eddies and turbulence in vegetation canopies: the mixing-layer analogy. Bound Layer Meteor 78:351–382
21. Rotach MW (1993) Turbulence close to a rough urban surface, part I: Reynolds stress. Bound Layer Meteor 65:1–28
22. Watanabe T (2004) Large-eddy simulation of coherent turbulence structures associated with scalar ramps over plant canopies. Bound Layer Meteor 112:307–341
23. Xie ZT, Coceal O, Castro IP (2008) Large-eddy simulation of flows over random urban-like obstacles. Bound Layer Meteor 129:1–23
24. Xie ZT (2011) Modelling street-scale flow and dispersion in realistic winds—towards coupling with mesoscale meteorological models. Bound Layer Meteor 141:53–75